An Enhanced Hybrid Battery Model

Taesic Kim, *Member, IEEE*, Wei Qiao, *Senior Member, IEEE,* and Liyan Qu, *Senior Member, IEEE*

***Abstract*—A high-fidelity battery model capable of accurately predicting real-time battery behavior for various operating conditions is crucial for the design and operation of battery-powered systems. Based upon a prior work of the authors, this paper proposes an enhanced hybrid battery model to provide accurate predictions for the runtime behaviors of rechargeable electrochemical battery cells under various ambient temperatures and charge/discharge current conditions. The proposed battery model is validated by simulation and experimental studies for lithium-ion battery cells in various current and temperature conditions. The proposed battery model is computationally effective for design, simulation, condition monitoring, and power management of various battery systems.**

***Index Terms*—Battery model, nonlinear capacity effect, nonlinear open circuit voltage (OCV), state of charge (SOC), temperature effect**

I. Introduction

RECHARGEABLE electrochemical batteries, such as lithium-ion batteries, have been used in various electrical systems, e.g., renewable energy systems, electric-drive vehicles, commercial electronics, etc. A battery-powered system requires a properly designed battery management system (BMS) to ensure the safety, reliability, and optimal performance of the battery. The performance of a BMS relies on a high-fidelity battery model to monitor the conditions, such as the state of charge (SOC), state of health (SOH), and state of power (SOP), of the battery in real time and optimally control the charge and discharge of the battery to prolong the battery life and usage and reduce the risk of overcharge and over-discharge [1]. Battery models have been used for various applications [2] such as battery health monitoring [1], optimal sizing of battery energy storage systems for electric vehicles [3], and stability analysis and dynamic simulation for microgrids [4]. To meet the requirements of these applications, the battery model should be able to accurately capture various nonlinear capacity effects, such as the rate capacity and recovery effects, and dynamic current-voltage (I-V) characteristics of the battery. The nonlinear capacity effects and dynamic I-V characteristics strongly depend on runtime factors, such as the temperature, the current rate (i.e., C-rate), and the direction of the current. In addition, a balance between the accuracy and complexity of the battery model should be considered for real-time execution.

The widely used battery models characterizing the runtime behaviors of electrochemical batteries can be classified into two categories: electrochemical models and electrical circuit models. The electrochemical models use complex nonlinear partial differential equations (PDEs) to describe the electrochemical physics of batteries, such as the concentration of ions in the electrodes and electrolyte [5]. The electrochemical models are the most accurate models. However, establishing these models requires the detailed knowledge of the battery chemical processes and the identification of a large number of parameters, which makes the models difficult to configure. Moreover, it is difficult to use electrochemical models for real-time applications due to the high complexity and intensive computation requirement. Therefore, the electrochemical models are more feasible for offline battery design and analysis. Some recently developed electrochemical models used many approximations and linearization methods to reduce the computational complexity [6]-[10]. However, they are still too complex for real-time BMS applications and efforts are needed to further reduce their computational complexity.

The electrical circuit models use equivalent electrical circuits to capture the I-V characteristics of batteries and have lower computational cost than electrochemical models. The structure and order (i.e., the number of resistor, capacitor, and inductor components) of an electrical circuit model depends on the desired model accuracy and the available test equipment used to extract the model parameters [11]. An electrical circuit model can be constructed as a frequency-domain model (e.g., the Randle's circuit model [12]) whose parameters can be obtained using an electrochemical impedance spectroscopy, or a time-domain model [13] whose parameters can be obtained by fitting the measured pulsed-current discharge/charge behaviors of the battery.

A comparison of various electrical circuit models was presented in [14]. The traditional electrical circuit models did not integrate the battery nonlinear capacity behaviors, leading to an inaccurate prediction of the runtime SOC [15]. The fidelity of the traditional electrical circuit models can be improved by making the model parameters dependent on several factors, such as SOC, C-rate [16], temperature and aging [17] of the battery. For example, an enhanced electrical circuit model was introduced in [15] by using the Rakhmatov's diffusion model [18] to characterize the nonlinear capacity effect. Recently, the authors developed a hybrid battery model [19] by replacing the Rakhmatov's diffusion model with a kinetic battery model (KiBaM) [20], which has a lower

This work was supported in part by the U.S. National Science Foundation under Grants IIP-1414393 and CMMI-1663562.

T. Kim is with the Department of Electrical Engineering and Computer Science, Texas A&M University–Kingsville, Kingsville, TX 78363 USA (e-mail: taesic.kim@tamuk.edu).

W. Qiao and L. Qu are with the Department of Electrical and Computer Engineering, University of Nebraska–Lincoln, Lincoln, NE 68588-0511 USA (e-mail: wqiao3@unl.edu; lqu2@unl.edu).

computational cost and the feature of simple implementation and, therefore, is more suitable for real-time BMS. However, the existing electrical circuit battery models with the nonlinear capacity effects only considered the discharge mode at a certain ambient temperature, e.g., the room temperature.

This paper extends the work of [19] to propose an enhanced hybrid battery model, which is capable of capturing accurate runtime SOC and I-V dynamics of batteries in both charge and discharge modes of operation and various ambient temperature conditions. On the contrary, the prior model in [19] was only developed for the discharge mode operation at the room temperature. Moreover, the proposed battery model includes a new runtime SOC estimation module, which requires less information, has a lower computational cost, and can be more easily implemented in a digital system or a simulation platform such as MATLAB/Simulink than that in [19]. Compared to the KiBaM in [20], the nonlinear open circuit voltage (OCV) effect is considered and temperature/current-dependent parameters are used in the proposed battery model. The model is effective for design, simulation, condition monitoring, and power management of various battery systems due to the good balance between accuracy and complexity among the existing battery models as well as a simple model extraction method. The proposed battery model is validated by extensive simulation and experimental studies for cylindrical lithium-ion battery cells.

The remainder of the paper is organized as follows. Section II presents the relationship between the nonlinear capacity and OCV effects and the KiBaM as the related work. Section III presents the proposed enhanced hybrid battery model. Section IV presents the model extraction method for the proposed battery model. Section V provides simulation and experimental results to validate the proposed battery model. Finally, Section VI concludes the paper and briefly discusses the future work.

II. Related Work

A. Nonlinear Capacity and OCV Effects

A rechargeable electrochemical battery cell consists of an anode and a cathode placed in an electrolyte medium. The current through the cell is generated by the electrochemical reactions at the electrode-electrolyte interface. The battery capacity depends nonlinearly on its current profile due to two nonlinear capacity effects: the rate capacity effect and the recovery effect. The rate capacity effect is that less charge can be drawn from a battery as the current rate of discharge increases due to a higher concentration gradient caused by the slow diffusion process at the active reaction site. This results in a lower capacity compared with the battery discharged with a lower current rate [19]. However, the unavailable charge due to the high gradient of concentration still remains in the battery if the thermal dissipation and self-discharge are neglected [19]. The unavailable charge will become available after a period with no or a low current due to the reduced gradient of concentration. This is the recovery effect.

The nonlinear capacity effects were originally defined and observed in the discharge process. This paper assumes that the rate capacity effect in the charge mode is that less charge can be stored into a battery as the current rate of charge increases due to a higher concentration gradient, which results in a lower charge acceptance compared with the battery charged with a lower current rate. The charge acceptance is the ability of the battery to accept charge [21]. During charging there is a limitation of lithium-ion insertion into the graphite layers of the anode (i.e., intercalation) due to the low ion conductivity and slow diffusion process in a lithium-ion battery cell. The limitation of lithium-ion intercalation deteriorates charge acceptance. However, the charge acceptance will be recovered if the battery relaxes. This can be explained as the recovery effect in the charge mode. If the charge current through the battery is too high in the high SOC region (e.g., SOC > 80%), it will cause surplus ions being deposited on the anode in the form of lithium metal. This phenomenon is called lithium plating [22] and will result in a loss of charge and heat dissipation. A part of the charge lost in the lithium plating process is irreversible. The lithium plating will become more significant at a lower temperature [22], causing a lower charge acceptance.

The nonlinear capacity effects cause a nonlinear OCV response (or effect). The time-domain responses of the terminal voltage (V_{cell}), OCV (Voc), and equilibrium OCV (Voc_{eq}) of a lithium-ion battery cell discharged and charged using a pulsed current profile are shown in Fig. 1, where Voc_{eq} is the steady-state terminal voltage of the battery cell; while Voc depends on the history of the battery usage due to the slow, long-term diffusion process during the operation. These voltage responses clearly show the nonlinear OCV effect as a consequence of the nonlinear capacity effects, namely, the Voc

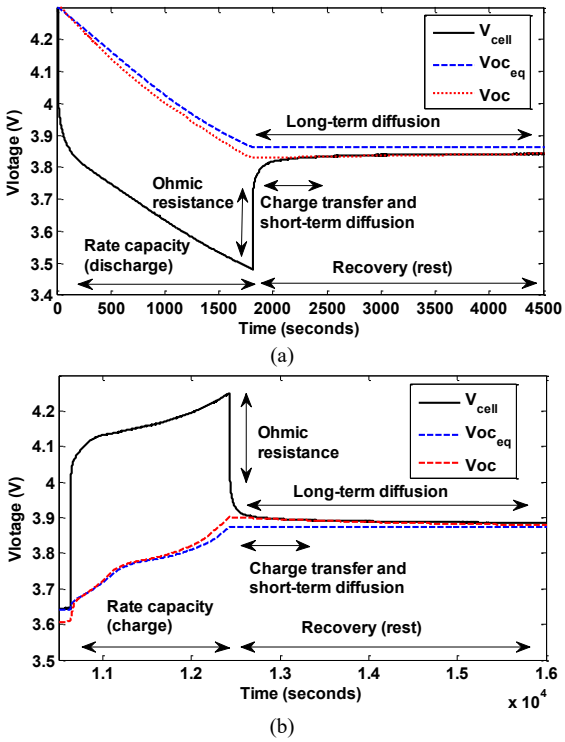

Fig. 1. Time-domain responses of the terminal voltage, OCV, and equilibrium OCV showing the nonlinear capacity and OCV effects of a lithium-ion battery cell with a pulsed current in the (a) discharge mode and (b) charge mode.

is smaller/larger than the Voc_{eq} due to the rate capacity effect in the discharge/charge process, and then rises up/falls down to converge to the Voc_{eq} slowly due to the recovery effect.

B. Simple Expression of the KiBaM

This paper utilizes two forms of the SOC: a transient SOC (SOC_T) and an equilibrium SOC (SOC_E). The SOC_T is the state of available capacity; and the SOC_E is the state of usable capacity. The usable capacity is the charge stored in the battery and can be calculated by using the Coulomb counting method while neglecting the nonlinear capacity effects. The available capacity is the charge that can be supplied by the battery [19], which depends on the current and nonlinear capacity effects of the battery. Both SOCs offer useful information in this paper. The SOC_T is the actual real-time SOC and can be used for runtime prediction (e.g., the remaining end of discharge time and end of charge time) of the battery. The SOC_E is used to estimate the maximum capacity of the battery [23].

The KiBaM is a model well suited for capturing the nonlinear capacity effects of batteries. A detailed description of the KiBaM can be found in [19] and [20]. In the KiBaM [20], it is assumed that a battery has two charge wells, and the charge is distributed with a capacity ratio c ($0 < c < 1$) between the two wells, as shown in Fig. 2. In the discharge mode, the available charge well delivers charge directly to the load; while the bound charge well supplies charge only to the available charge well through a valve v. The rate of charge flowing from the bound charge well to the available charge well depends on v and the difference in the heights of the two wells, h_1 and h_2, where h_1 is related to the SOC_T of the battery. $h_{1,max}$ and $h_{2,max}$ are the maximum heights of the available and bound charge wells, respectively. The battery is fully discharged when h_1 becomes zero. The changes of the total charges y_1 in the available charge well and y_2 in the bound charge well are expressed as [20]:

$$\begin{cases} \dfrac{dy_1(t)}{dt} = -i_B(t) + v[h_2(t) - h_1(t)] \\ \dfrac{dy_2(t)}{dt} = -v[h_2(t) - h_1(t)] \end{cases} \tag{1}$$

where $i_B(t)$ is the battery current, which is positive if the battery is operated in the discharge mode. The height difference, $\delta = h_2 - h_1$, between the two wells plays an important role in obtaining the nonlinear capacity variation in the discharge mode.

Based on the KiBaM, an enhanced Coulomb counting algorithm was derived in [19] for SOC_T prediction:

$$\begin{cases} SOC_T(t) = \dfrac{C_{available}}{C_{\max}} = SOC_T(t_0) - \dfrac{\int i_B(t)dt + C_{unavailable}(t)}{C_{\max}} \\ C_{unavailable}(t) = (1-c)\cdot\left[\delta(t_0)e^{-k'(t-t_0)} + \dfrac{i_B(k)}{c}\cdot\dfrac{1-e^{-k'(t-t_0)}}{k'}\right] \end{cases} \tag{2}$$

where t_0 is the beginning time of the SOC_T prediction, k' (= $v/[c(1-c)]$) is a constant diffusion rate; $C_{\max}$, $C_{available}$ and $C_{unavailable}$ are the maximum, available and unavailable capacities of the battery, respectively.

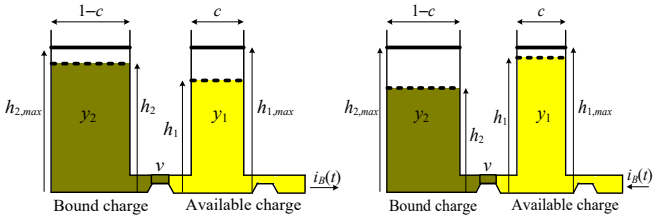

Fig. 2. The KiBaM in the: (a) discharge mode and (b) charge mode.

SOC_E can be calculated by omitting the term $C_{unavailable}$ in (2):

$$SOC_E(t) = \frac{C_{usable}}{C_{\max}} = SOC_E(t_0) - \frac{\int i_B(t)dt}{C_{\max}} \tag{3}$$

where C_{usable} is the usable capacity.

In this paper, the formula of the KiBaM regarding the SOCs is derived. First, $dy_1(t)/dt$ in (1) can be expressed as:

$$\frac{dy_1(t)}{dt} = -k'[1-c]y_1(t) + k'\cdot c\cdot y_2(t) - i_B(t) \tag{4}$$

where $y_1 = c\cdot h_1$ and $y_2 = (1\text{-}c)\cdot h_2$. By using $SOC_E = (y_1+y_2)/C_{\max}$, (4) can be reformulated as follows:

$$\frac{dy_1(t)}{dt} = -k'y_1(t) + k'\cdot c\cdot C_{\max}SOC_E - i_B(t) \tag{5}$$

Since $y_1 = c\cdot C_{\max}\cdot SOC_T$, the following can be obtained from (5):

$$\frac{dSOC_T(t)}{dt} = k'SOC_E - k'SOC_T - \frac{i_B(t)}{c\cdot C_{\max}} \tag{6}$$

By combining (6) and the differential equation of (3), the KiBaM regarding the two SOCs can be expressed as:

$$\begin{bmatrix} \dfrac{dSOC_E(t)}{dt} \\ \dfrac{dSOC_T(t)}{dt} \end{bmatrix} = \begin{bmatrix} 0 & 0 \\ k' & -k' \end{bmatrix}\cdot\begin{bmatrix} SOC_E(t) \\ SOC_T(t) \end{bmatrix} + \begin{bmatrix} \dfrac{-1}{C_{\max}} \\ \dfrac{-1}{c\cdot C_{\max}} \end{bmatrix}\cdot i_B(t) \tag{7}$$

It should be noted that the KiBaM used in this paper focuses on battery capacity, which is a measure of the charge stored by the battery; while energy-focused KiBaMs can be found in [24], [25].

III. The Proposed Enhanced Hybrid Battery Model

The proposed enhanced hybrid model consists of two parts: a runtime SOC prediction module and an electrical circuit, as seen in Fig. 3. The runtime SOC prediction module is designed based on (7) to capture the nonlinear capacity variation; while the electrical circuit is designed to capture the I-V characteristics of batteries. The parameters of the proposed battery model are functions of the current direction D, SOC_T, SOC_E, C-rate I, and ambient temperature T of the battery and updated online during battery operation. Thus, the proposed battery model is capable of capturing the comprehensive runtime behavior of a battery under any operating conditions. To facilitate real-time system applications, a discrete-time version of the model is developed.

A. The Proposed Runtime SOC Prediction Module

Using the first-order forward Euler method, the discrete-time form of (7) is given below:

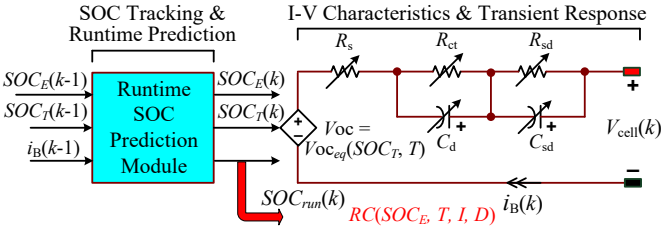

Fig. 3. The proposed hybrid battery model.

$$\begin{bmatrix} SOC_E(k+1) \\ SOC_T(k+1) \end{bmatrix} = \begin{bmatrix} 1 & 0 \\ k'T_S & (1-k'T_S) \end{bmatrix} \cdot \begin{bmatrix} SOC_E(k) \\ SOC_T(k) \end{bmatrix} + \begin{bmatrix} \frac{-T_S}{C_{\max}} \\ \frac{-T_S}{c \cdot C_{\max}} \end{bmatrix} \cdot i_B(k) \tag{8}$$

where k denotes the time index and T_S is the sampling period. In [19], SOC_T was used to represent the actual real-time SOC in the discharge mode. However, it will be inappropriate to use SOC_T in the charge mode because the SOC_T (or $C_{available}$) calculated by (2) will be larger than the SOC_E (or C_{usable}) calculated by (3); while by definition, SOC_T should always be smaller than or equal to SOC_E. Therefore, using SOC_T in the charge mode will inaccurately indicate that the charge stored in the battery is more than that actually stored. To solve this problem, a runtime SOC, SOC_{run}, is proposed. The SOC_{run} is the same as SOC_T when SOC_T is smaller than SOC_E in the discharge mode; while the SOC_{run} is the same as SOC_E when SOC_T is larger than SOC_E, which usually happens in the charge mode. In addition, considering the limit of the charge acceptance in the charge mode, the SOC_{run} should be limited to 1. This issue was not considered in the original KiBaM in [20]. Therefore, the SOC_{run} is expressed as:

$$SOC_{run} = \min[SOC_T, SOC_E, 1] \tag{9}$$

In this paper, the influence of the ambient temperature on the KiBaM is investigated more explicitly than that in [19] and [20]. According to the Arrhenius equation and experiments, the parameters of KiBaM are expressed as the following empirical functions of the ambient temperature T in Kelvin (K):

$$\begin{cases} C_{\max}(T) = a_0 e^{-a_1\left(\frac{1}{T-a_2}-\frac{1}{T_{ref\_L}-a_2}\right)} \\ k'(T) = a_3 e^{a_4(T-T_{ref\_L})} + a_5 \\ c(T) = a_6 e^{-\left(\frac{T-a_7}{a_8}\right)^2} \end{cases} \tag{10}$$

where T_{ref_L} is equal to 273.15 K (i.e., 0 °C) and a_0, ⋯, a_8 are coefficients.

B. The Proposed Electrical Circuit

The electrical circuit describes the I-V characteristics and transient response of a battery, where a temperature-dependent voltage-controlled voltage source, $Voc_{eq}(SOC_T, T)$, i.e., Voc in Fig. 1, is used to bridge the SOC_T to the nonlinear OCV and characterizes the long-term diffusion effect of the battery; the series resistance R_s characterizes the instantaneous voltage drop/rising response V_s at the beginning and end of the discharge/charge process of the battery due to the resistances of the electrode, electrolyte, separator, contact, etc.; other resistances and capacitances characterize the transient responses of the battery, including the charge transfer voltage response V_{ct} due to the double-layer capacitance C_d and charge transfer resistance R_{ct} as well as the short-term diffusion voltage response V_{sd} due to the short-term diffusion capacitance C_{sd} and resistance R_{sd}; and V_{cell} represents the terminal voltage of the battery. All of the sources contributing to the voltage response of the battery are shown in Fig. 1. A discrete-time version of the electrical circuit model is expressed as follows:

$$Voc = Voc_{eq}(SOC_T, T) = Voc_{eq}(SOC_T, T_{ref}) \cdot K_{VOC}(SOC_T, T) \tag{11}$$

$$V_{cell}(k) = Voc_{eq}(SOC_T, T) - R_s \cdot i_B(k) - V_{ct}(k) - V_{sd}(k) \tag{12}$$

$$\begin{bmatrix} V_{ct}(k) \\ V_{sd}(k) \end{bmatrix} = \begin{bmatrix} e^{\frac{-T_s}{\tau_S}} & 0 \\ 0 & e^{\frac{-T_s}{\tau_L}} \end{bmatrix} \cdot \begin{bmatrix} V_{ct}(k-1) \\ V_{sd}(k-1) \end{bmatrix} + \begin{bmatrix} R_{ct}(1-e^{\frac{-T_s}{\tau_S}}) \\ R_{sd}(1-e^{\frac{-T_s}{\tau_L}}) \end{bmatrix} \cdot i_B(k) \tag{13}$$

where K_{VOC} is a correction coefficient for the temperature effect; $\tau_S = R_{ct} \cdot C_d$; and $\tau_L = R_{sd} \cdot C_{sd}$.

The resistor-capacitor (RC) network parameters in Fig. 3 are functions of SOC_E, C-rate I, current direction D, and ambient temperature T. The formulas of the RC parameters will be given in Section IV.

IV. Model Extraction

Numerous experiments have been conducted for Samsung's ICR18650-28A cylindrical lithium-ion battery cells to validate the proposed model. The ICR18650-28A is a 2.8-Ah $LiMn_2O_4$ battery cell with the nominal voltage of 3.75 V. In the experiments, four battery cells are randomly chosen and tested in a Sun Electronic System EC12 temperature chamber. The voltages and currents of the four test cells are measured by a CADEX C8000 battery tester simultaneously. The parameters of the proposed battery model (i.e., $C_{delivered}$, $C_{\max}$, c, k', Voc_{eq}, R_s, R_{ct}, C_d, R_{sd}, and C_{sd}) are extracted from the test results of each cell. Then, the average values of each parameter (e.g., $C_{\max}$) extracted from the test results of the four cells are used to determine the coefficients of the corresponding empirical equation such as (10) via curve fitting. The coefficients of the empirical equations are influenced by many factors, such as the C-rate, current direction, and ambient temperature. These coefficients are identified using curve fitting through constant discharge current and pulsed discharge/charge current tests at three different ambient temperature conditions: low temperature (0 °C or 273.15 K, which is the lowest operating temperature of the battery), room temperature (23 °C or 296.15 K), and high temperature (40 °C or 313.15 K). Before the tests, the battery cells are fully charged using the constant current constant voltage (CCCV) charge method, where the charge cutoff voltage in the constant current mode is 4.3 V and the charge cutoff current in the constant voltage mode is 0.01C (i.e., i_B = 0.028 A). In each test, the fully charged battery cells are placed in the temperature chamber for four hours for the cells to reach a thermal equilibrium (i.e., the internal temperature is the same as the ambient temperature) before testing the cells.

A. Parameters of the Runtime SOC Prediction Module

The parameters of the runtime SOC prediction module are identified using constant discharge current tests. Specifically, the maximum capacity, $C_{\max}$, is extracted by discharging the fully-charged cell with a small constant current (e.g., 0.05C) until it is fully discharged, where the cell voltage reaches the discharge cutoff voltage of 3 V. Then, the parameters c and k' are obtained by curve fitting using the following equation [26]:

$$C_{delivered}(I) = \frac{C_{\max} k' c L(I)}{(1 - e^{-k'L(I)} + c \cdot (k'L(I) - 1 + e^{-k'L(I)})} \quad (14)$$

where I is a vector of constant discharge current rate (i.e., C-rate) from 0.1C to 1.8C with an increment of 0.2C; $C_{delivered}(I)$ and $L(I)$ are the vectors of the delivered capacity and the end of discharge time corresponding to I, respectively, where $C_{delivered}$ is the maximum capacity that can be delivered by a fully-charged cell, i.e., the maximum available capacity. The value of $C_{delivered}$ at a certain constant discharge current i_B ($i_B \in I$) is obtained by discharging the fully-charged cell with i_B until the cell voltage reaches the discharge cutoff voltage of 3 V and using the following equation.

$$C_{delivered} = i_B L(i_B) \quad (15)$$

Fig. 4(a) shows the values of $C_{delivered}$ calculated using (15) and the corresponding fitted $C_{delivered}$ curves using (14) at three different ambient temperature conditions. The extracted average values of $C_{\max}$, c and k' from the four battery cells for the three different ambient temperature conditions and the fitted curves of these parameters as functions of the ambient temperature are plotted in Fig. 4(b)-(d), respectively. The values of the coefficients a_0–a_8 in (10) obtained from the curve fitting are listed in Table I. It is observed that the values of k' and $C_{\max}$ increase with ambient temperature since most chemical processes in the cell are sped up at higher temperatures. However, the temperature effect on the parameter c is not consistent with the other two parameters. The parameter c has the highest value at the room temperature.

TABLE I
THE COEFFICIENTS OF THE EMPIRICAL EQUATIONS OF THE RUNTIME SOC PREDICTION MODULE PARAMETERS AND OCV FOR THE TEST BATTERY CELLS

a_0	9801	a_1	36.49	a_2	479.9	a_3	4.463e-6
a_4	0.1768	a_5	6.226e-4	a_6	0.8819	a_7	292.6
a_8	28.27	a_9	-0.1364	a_{10}	61.94	a_{11}	3.616
a_{12}	1.095	a_{13}	-2.949	a_{14}	4.295	a_{15}	-1.765
a_{16}	150.8	a_{17}	33.17	a_{18}	8.67e-5	a_{19}	1.025

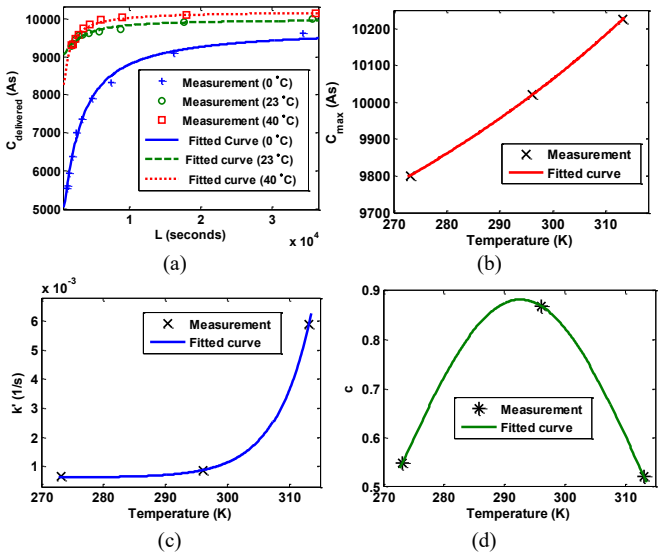

Fig. 4. The measured or estimated values and corresponding fitted curves of (a) $C_{delivered}$ as a function of $L(I)$ at three different ambient temperature conditions from a battery cell as well as averaged (b) $C_{\max}$, (c) k', and (d) c as functions of temperature from the four battery cells.

B. Electrical Circuit Parameters

The electrical circuit parameters (Voc and RC parameters) of the proposed battery model are extracted by using a pulsed current discharge and charge test cycle under the three ambient temperature conditions, where the pulsed current discharge test is firstly conducted and followed by the pulsed current charge test once the cell voltage reaches the discharge cutoff voltage. Each current pulse lasts for a period during which the SOC_E of the battery cell decreases or increases by 5% in the discharge or charge mode, respectively. Before the test, the value of $C_{\max}$ has been extracted for accurate SOC_E calculation to account for the change in $C_{\max}$ caused by the ambient temperature variation.

The discharge and charge equilibrium OCVs are the terminal voltage measured at the end of the rest period of each current pulse during the pulsed current discharge and charge test, respectively, where the rest period should be long enough, e.g., 3 hours at 40 °C, 6 hours at 23 °C, and 9 hours at 0 °C. The pulsed current discharge and charge test cycle is conducted with a cell current of 0.6C (i.e., 1.68 A) to extract the equilibrium OCVs. Fig. 5(a) shows the Voc_{eq}, which is the average value of the discharge and charge equilibrium OCVs,

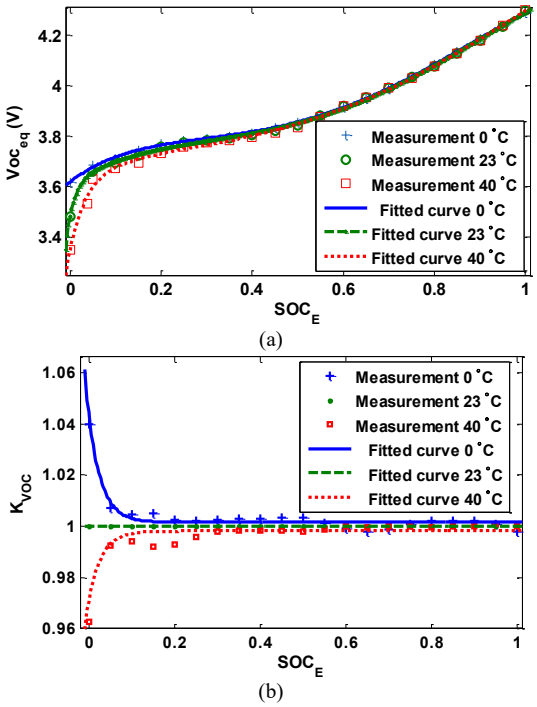

Fig. 5. Measured average values and fitted curves obtained from the four battery cells at the ambient temperatures of 0 °C, 23 °C, and 40 °C: (a) Voc_{eq} and (b) K_{VOC} vs. SOC_E.

versus SOC_E for the test cell under the ambient temperatures of 0 °C, 23 °C, and 40 °C. The Voc_{eq} strongly depends on SOC and temperature when the SOC is less than 10%. In addition, the difference between the discharge and charge equilibrium OCVs is less than 5 mV. Therefore, the hysteresis effect [27] can be ignored.

The empirical equation of the Voc_{eq} at the room temperature T_{ref}, which is called the reference Voc_{eq}, can be obtained using the following equation [19]:

$$Voc_{eq}(SOC_E, T_{ref}) = a_9 e^{-a_{10}SOC_E} + a_{11} + a_{12}SOC_E + a_{13}SOC_E^{\,2} + a_{14}SOC_E^{\,3} + a_{15}SOC_E^{\,4} \quad (16)$$

where T_{ref} = 296.15 K and a_9, ⋯, a_{15} are coefficients. Then, the correction coefficient for the temperature effect, K_{VOC} shown in Fig. 5(b), can be obtained as follows from the Voc_{eq} values measured at the low and high ambient temperatures and the measured reference Voc_{eq} values:

$$K_{VOC}(SOC_E, T) = \frac{Voc_{eq}(SOC_E, T)}{Voc_{eq}(SOC_E, T_{ref})} \quad (17)$$

The empirical equation of K_{VOC} is then formulated as:

$$K_{VOC}(SOC_E, T) = a_{16}\left(\frac{1}{T} - \frac{1}{T_{ref}}\right) \cdot e^{-a_{17}SOC_E} - a_{18}T + a_{19} \quad (18)$$

The coefficients a_9–a_{18} in (16) and (18) are obtained from curve fitting and listed in Table I.

As described by (16)-(18), the SOC_E is used to facilitate the characterization of the Voc_{eq} at T_{ref} and K_{VOC} in the offline model extraction process by neglecting the nonlinear OCV effect. Then, when using the proposed battery model, the Voc is estimated by using (11), where the SOC_E in (16) and (18) is replaced with the SOC_T to consider the nonlinear OCV effect.

Then, all of the RC parameters are extracted from the impedance voltage response (i.e., $V_{impedance} = |V_{cell} - Voc_{eq}(SOC_T, T)|$) measured in each pulse of the pulsed current discharge and charge test cycle. Fig. 6 depicts a typical curve of the $V_{impedance}$ response in one discharge current pulse during which the SOC_E of the battery cell decreases by 5%, where the window contains the data in a certain interval of the rest period used for the extraction of the RC parameters via curve fitting. In this paper, a 10-minute fitting window is used by assuming that the RC parameters related to the charge transfer and short-term diffusion can be observed within a 10-minute rest period. The RC parameters are expressed as functions of SOC_E so that the nonlinear capacity effect mainly influences the nonlinear OCV effect as discussed in Section II.A.

According to (12), the instantaneous voltage drop/rise when the discharge/charge completed is related with R_s, which can be expressed by the following equation:

$$R_s = \frac{V_s}{|i_B|} = \frac{V0 - V1}{|i_B|} \quad (19)$$

where $V0$ and $V1$ are obtained from Fig. 6. Based on (8) and (9), the following equation is obtained to estimate the RC parameters:

$$V_{ct}(k) + V_{sd}(k) = a \cdot e^{-b \cdot k} + c \cdot e^{-d \cdot k} + e \quad (20)$$

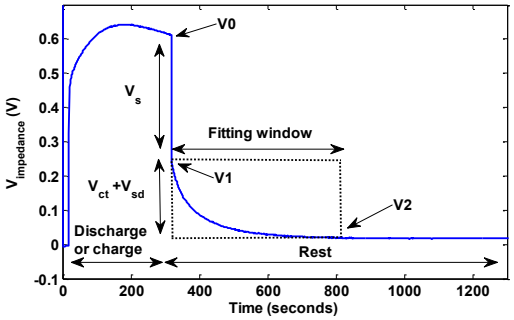

Fig. 6. The curve of a typical impedance voltage response in the condition of 0.6C pulsed current discharge and 0 °C ambient temperature for the extraction of the RC parameters of the proposed battery model.

where k = 1, ⋯, 600; and $e = V2$ in Fig. 6. The coefficients a, b, c and d are determined by using nonlinear least-square curve fitting. The RC parameters are then calculated as [19]:

$$R_{ct} = a/|i_B|,\ C_d = 1/(R_{ct} \cdot b),\ R_{sd} = c/|i_B|,\ C_{sd} = 1/(R_{sd} \cdot d) \quad (21)$$

Since the RC parameters depend on the C-rate I, SOC_E, ambient temperature T, and current direction of the battery cell, numerous experiments are conducted to extract the RC parameters using the pulsed current discharge and charge test cycle with different values of I and T. Then, the empirical equations of the RC parameters are derived by combining polynomial and exponential curve fitting. First, the empirical equations as functions of SOC_E and I for the discharge mode are derived at three different I values of 0.2C, 0.6C, and 1C at the room temperature (i.e., the reference temperature).

$$\begin{cases} R_{s,d}(SOC_E, I) = (a_{d0} - a_{d1}I)e^{-a_{d2}SOC_E} + a_{d3} + a_{d4}I + a_{d5}SOC_E + a_{d6}SOC_E^{\,2} + a_{d7}SOC_E^{\,3} \\ R_{ct,d}(SOC_E, I) = (b_{d0} - b_{d1}I)e^{-b_{d2}SOC_E} + b_{d3} + b_{d4}I + b_{d5}SOC_E \\ R_{sd,d}(SOC_E, I) = (c_{d0} - c_{d1}I)e^{-c_{d2}SOC_E} + c_{d3} + c_{d4}I + c_{d5}SOC_E \\ C_{d,d}(SOC_E, I) = d_{d0}SOC_E + d_{d1}SOC_E^{\,2} + d_{d2}SOC_E^{\,3} + d_{d3} \\ C_{sd,d}(SOC_E, I) = e_{d0}e^{-e_{d1}SOC_E} + e_{d2} + e_{d3}I + e_{d4}I^2 \end{cases} \quad (22)$$

where the subscript d of each RC parameter indicates the discharge mode. Then, the temperature dependency is added to the expression of each RC parameter based on the Arrhenius equation, which changes (22) to:

$$\begin{cases} R_{s,d}(SOC_E, I, T) = R_{s,d}(SOC_E, I) \cdot (e^{-f_{d0}\Delta T} + f_{d1}SOC_E^{\,f_{d2}}\Delta T) + K_{LV} \\ R_{ct,d}(SOC_E, I, T) = R_{ct,d}(SOC_E, I) \cdot e^{f_{d3}\left(\frac{1}{T} - \frac{1}{T_{ref}}\right)} \\ R_{sd,d}(SOC_E, I, T) = R_{sd,d}(SOC_E, I) \cdot e^{f_{d4}\left(\frac{1}{T} - \frac{1}{T_{ref}}\right)} \\ C_{d,d}(SOC_E, I, T) = C_{d,d}(SOC_E, I) \cdot e^{f_{d5}\left(\frac{1}{T} - \frac{1}{T_{ref}}\right)} \\ C_{sd,d}(SOC_E, I, T) = C_{sd,d}(SOC_E, I) \cdot e^{f_{d6}\left(\frac{1}{T} - \frac{1}{T_{ref}}\right)} \end{cases} \quad (23)$$

where

$$K_{LV}(SOC_E, I, T) = f_{d7} e^{-f_{d8}(T - T_{ref\_L})}(e^{-f_{d9} SOC_E} - I^{f_{d10}}) \quad (24)$$

Due to the increase in the fitting error at low temperatures, an additional correction factor K_{LV} is added to the expression of $R_{s,d}$. All of the coefficients of the empirical equations of the RC parameter (22)-(24) are listed in Table II. The extracted values and the corresponding fitted curves of the RC parameters are shown in Fig. 7, where Fig. 7(a) illustrates the C-rate and SOC_E dependency of the RC parameters expressed by (22) and Fig. 7(b)-(f) shows the temperature dependency of the RC parameters expressed by (23)-(24) at the reference C-rate 0.6C. The fitting error of $R_{sd,d}$ with respect to the measurement at 0 °C increases significantly as the SOC exceeds about 0.6, as shown in Fig. 7(e). It indicates that the Arrhenius equation, which is commonly used to represent the dependence of the rate constant of a chemical reaction on the absolute temperature, may not be effective to represent the temperature dependence of some RC parameters of the battery at 0 °C due to the highly unexpected nonlinearity of the battery cell at the lowest operating temperature. However, since the fitting result of the series resistance $R_{s,d}$ at 0 °C is accurate over the entire SOC range, as shown in Fig. 7(b), and $R_{s,d}$ is the dominant resistance of the battery model, particularly at 0 °C, the relatively large fitting errors of $R_{sd,d}$ in the high SOC range at 0 °C will not significantly affect the accuracy of the proposed model for capturing the runtime behaviors of battery cells.

The empirical equations of the RC parameters and their coefficients for the charge mode are obtained from a similar process and are given in the Appendix.

V. Validation

The proposed battery model is constructed in MATLAB/Simulink by using the standard components from the Simulink toolbox. In the Simulink model, a "runtime SOC module" calculates the values of SOC_T, SOC_E, and SOC_{run} of the battery cell by taking into account its nonlinear capacity variation during the operation, and an "I detector" module tracks the change of the battery cell current i_B and converts it to the C-rate I. When the C-rate I or temperature exceeds the extreme values used to obtain the model, the Simulink model can still predict the runtime behaviors of the battery cell.

The parameters of the battery model are obtained from four ICR18650-28A $LiMn_2O_4$ battery cells by using the model extraction method described in Section IV. Simulation results obtained from the proposed battery model are compared with the experimental data for a randomly selected new ICR18650-28A cell in the low (0 °C), room (23 °C), and high (40 °C) temperature conditions using pulsed and random discharge and charge current profiles to validate the proposed battery model.

Fig. 8(b), (d) and (f) compare the terminal voltage responses obtained from simulations with the experimental results for the pulsed discharge/charge current profile shown in Fig. 8(a). The proposed model captures the dynamic voltage responses of the battery cell accurately in all current and temperature conditions. The maximum root mean square error (RMSE) of the cell terminal voltage predicted by the proposed model in the middle and entire SOC ranges during the test are only 23 mV or 1.77% and 31 mV or 2.4%, respectively, of the nominal terminal voltage variation range of 1.3 V (= 4.3−3 V), which occurs in the 0 °C condition, as shown in Fig 9(b). The maximum error of the cell terminal voltage predicted by the proposed model in the middle and entire SOC ranges are about 14.2 mV or 1.1% and 92 mV or 7.1%, respectively, of the nominal terminal voltage variation range, which occurs at 40 °C, as shown in Fig. 8(f). This is caused by relatively large fitting errors on the OCV-SOC curve for the SOC around 0.1 at 40 °C, as shown in Fig. 5(a). Moreover, by capturing the variations of the nonlinear capacity effects, the proposed model is able to

TABLE II
The Coefficients of the RC Parameter Expressions for the Test Cylindrical Lithium-Ion Cells in the Discharge Mode

a_{d0}	0.2904	a_{d1}	0.2521	a_{d2}	9.485	a_{d3}	0.1674
a_{d4}	-0.0100	a_{d5}	-0.1726	a_{d6}	0.1553	a_{d7}	-0.02982
b_{d0}	0.0664	b_{d1}	0.0558	b_{d2}	13.44	b_{d3}	0.01358
b_{d4}	5.48E4	b_{d5}	0.0134	c_{d0}	0.6882	c_{d1}	80.89
c_{d2}	0.0196	c_{d3}	7.354	c_{d4}	0.0841	c_{d5}	-6.686
d_{d0}	5528	d_{d1}	-10850	d_{d2}	6044	d_{d3}	550.5
e_{d0}	-3112	e_{d1}	17.1	e_{d2}	8058	e_{d3}	-9560
e_{d4}	14300	f_{d0}	0.0419	f_{d1}	0.0163	f_{d2}	0.25
f_{d3}	1554	f_{d4}	1835	f_{d5}	-771	f_{d6}	-1421
f_{d7}	39.85	f_{d8}	0.2993	f_{d9}	1.91e-3	f_{d10}	0.0022

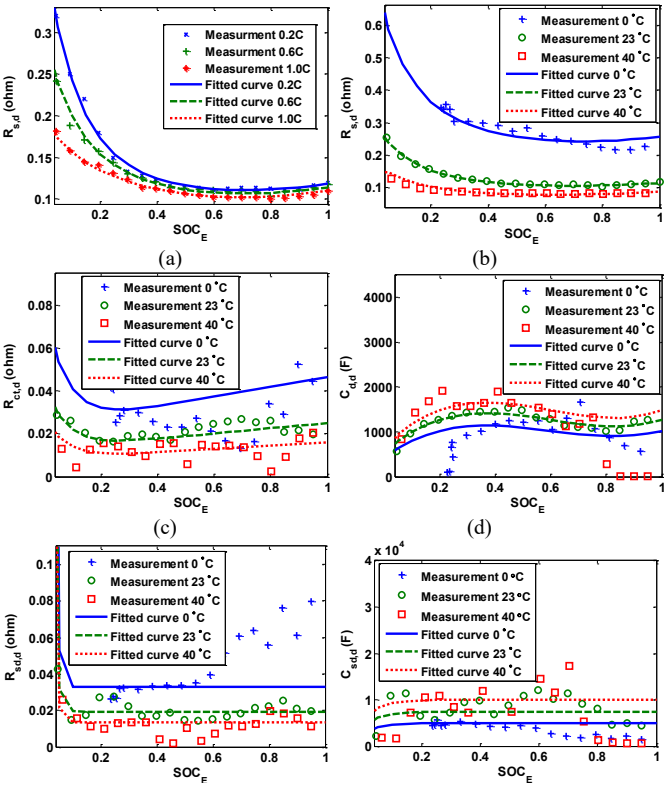

Fig. 7. The measurements and corresponding fitted curves of: (a) $R_{s,d}(SOC_E, I)$ at 23 °C, (b) $R_{s,d}(SOC_E, T)$ at 0.6C, (c) $R_{ct,d}(SOC_E, T)$ at 0.6C, (d) $C_{d,d}(SOC_E, T)$ at 0.6C, (e) $R_{sd,d}(SOC_E, T)$ at 0.6C, and (f) $C_{sd,d}(SOC_E, T)$ at 0.6C.

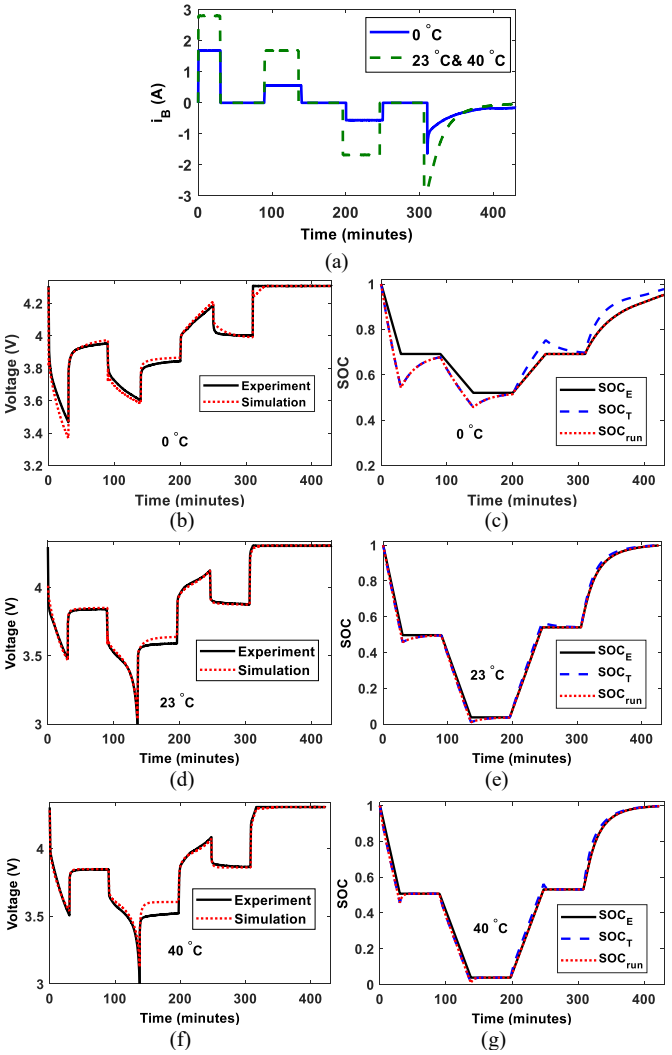

Fig. 8. Comparison of simulation and experimental results of the test battery cell with pulsed discharge and charge currents: (a) the pulsed current profiles, (b) the voltage response at 0 °C, (c) the estimated SOCs at 0 °C, (d) the voltage response at 23 °C, (e) the estimated SOCs at 23 °C, (f) the voltage response at 40 °C, and (g) the estimated SOCs at 40 °C.

accurately capture the remaining end of discharge time until SOC_{run} = 0 and the end of charge time until SOC_{run} = 1 of the single battery cell in different current and temperature conditions, as shown in Fig. 8(c), (e) and (g).

In contrast, the error bands of the state-of-the-art battery model presented in [17] are ±20 mV in the middle SOC range but increased to ±171 mV in the entire SOC range, which is much larger than the errors of the proposed battery model under different temperature conditions in the entire SOC range.

The proposed enhanced hybrid battery model is further validated by comparing with the hybrid battery model in [19] and experimental results for a randomly varied discharge and charge current profile, as shown in Fig. 9(a). The parameters of the hybrid battery model are listed in Table V in Appendix. Fig. 9(b)-(d) compares the corresponding terminal voltage responses of the cell obtained from the simulation models and experiment. The voltage responses predicted by the proposed model are always better than those predicted by the hybrid battery model in [19] at various temperature conditions,

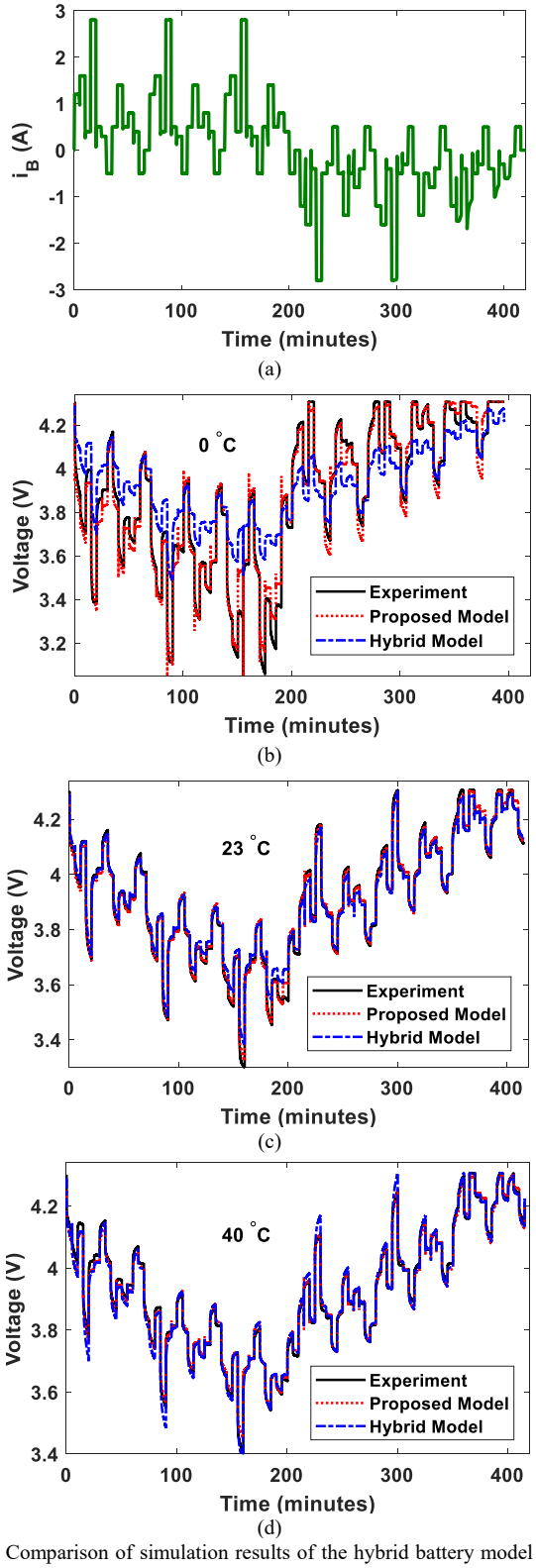

Fig. 9. Comparison of simulation results of the hybrid battery model in [19] and the proposed enhanced hybrid battery model with experimental results with (a) a randomly varied current profile at (b) 0 °C, (c) 23 °C, and (d) 40 °C.

particularly at the low temperature condition. Table III compares the RMSE results of the two battery models with respect to the experimental results at the three different temperature conditions. In the worst case at 0 °C, the RMSE of the voltage predicted by the proposed model is about 49.9 mV

TABLE III
RMSE RESULTS OF THE BATTERY MODELS IN FIG. 9

Temperature (°C)	0	23	40
Hybrid Battery Model [19] (mV)	188.9	27.3	19.4
Proposed Enhanced Hybrid Battery Model (mV)	49.9	14.1	14.4

or 3.8% of the nominal terminal voltage variation range, which is only 26% of the RMSE of the hybrid battery model in [19]. Although the RMSE values of the hybrid battery model are reduced significantly at 23 °C and 40 °C, they are still approximately 93.6% and 34.7% larger than the RMSE values of about 14.1 mV (or 1.08%) and 14.4 mV (or 1.1%) of the proposed model, respectively. These results show that the proposed model can capture the nonlinear capacity variations and dynamic I-V characteristics of lithium-ion batteries more accurately than the hybrid battery model in [19] under various currents and ambient temperatures.

It is expected that the proposed battery model can increase the accuracy of the electrical circuit models by only adding a discrete-time state-space equation (8) and several polynomial equations to the electrical circuit models. This indicates that once the model parameters are extracted, the computational complexity of the proposed battery model is similar to the electrical circuit models. Therefore, the proposed battery model has achieved a good balance between the electrical circuit models and the electrochemical models in terms of accuracy and computational cost.

VI. CONCLUSION AND FUTURE WORK

This paper has presented an enhanced hybrid battery model, which is capable of capturing dynamic I-V characteristics and nonlinear capacity variations of battery cells under various runtime operating conditions. The proposed battery model has been implemented in MATLAB/Simulink for a cylindrical lithium-ion cell. Simulation results of the proposed battery model have been compared with those of the hybrid battery model in [19] and experimental results. Results have validated that the proposed model can accurately capture the runtime behaviors of the battery cells under various temperature and charge/discharge current conditions.

In practical applications that use a battery pack with multiple cells, the proposed battery model can be copied with each copy representing a single cell if the user is interested in the runtime behaviors of individual cells that may have state imbalance, or the proposed battery model can be used to represent the entire battery pack if the state imbalance between different cells is neglected and the user is only interested in the terminal behavior of the battery pack for the co-simulation with other electrical circuits. In the future work, the low temperature effect, aging effect, and model complexity will be investigated to develop empirical equations with better fitting accuracy and minimum degree-of-freedom for the proposed battery model.

VII. APPENDIX

The empirical equations of the RC parameters of the proposed battery model for the charge mode are the following:

TABLE IV
THE COEFFICIENTS OF THE RC PARAMETER EXPRESSIONS FOR THE TEST CYLINDRICAL LITHIUM-ION CELLS IN THE CHARGE MODE

a_{c0}	-0.1233	a_{c1}	0.191	a_{c2}	-0.1295	a_{c3}	0.1556
a_{c4}	0.4472	a_{c5}	0.1515	a_{c6}	0.3407	a_{c7}	0.03541
a_{c8}	-0.0577	a_{c9}	-0.0412	b_{c0}	2.68e-5	b_{c1}	-5.007
b_{c2}	0.0230	b_{c3}	-1.16e-3	b_{c4}	-0.0312	b_{c5}	0.6319
c_{c0}	1.14e-5	c_{c1}	-8.112	c_{c2}	0.0122	c_{c3}	0.5869
c_{c4}	0.7105	c_{c5}	0.4211	c_{c6}	3098	d_{c0}	-4788
d_{c1}	0.0202	d_{c2}	5965	e_{c0}	-246.9	e_{c1}	3
e_{c2}	9856	e_{c3}	1338				

TABLE V
THE COEFFICIENTS OF THE HYBRID BATTERY MODEL IN [19] FOR THE TEST CYLINDRICAL LITHIUM-ION CELLS

a_{h0}	-0.1364	a_{h1}	61.94	a_{h2}	3.616	a_{h3}	1.095
a_{h4}	2.949	a_{h5}	4.295	a_{h6}	-1.765	b_{h0}	32.73
b_{h1}	207	b_{h2}	0.2382	b_{h3}	-0.5495	b_{h4}	-0.7608
b_{h5}	-0.3408	c_{h0}	0.0782	c_{h1}	14.95	c_{h2}	0.0309
d_{h0}	-900	d_{h1}	8.378	d_{h2}	1069	e_{h0}	0.05672
e_{h1}	19.37	e_{h2}	0.01851	f_{h0}	-9052	f_{h1}	6.73
f_{h2}	22440	c	0.8681	k'	0.0006541		

$$
\begin{cases}
R_{s,c}(SOC_E, I, T) = (a_{c0}SOC_E + a_{c1}SOC_E{}^2 + a_{c2}SOC_E{}^3 + a_{c3}) \\
\qquad \cdot (a_{c4}I^{-a_{c5}} + a_{c6}) \cdot (e^{-a_{c7}\Delta T} + a_{c8}SOC_E{}^{a_{c9}}\Delta T) \\
R_{ct,c}(SOC_E, I, T) = (b_{c0}e^{-b_{c1}SOC_E} + b_{c2}) \cdot (e^{-b_{c3}\Delta T} + b_{c4}SOC_E{}^{b_{c5}}\Delta T) \\
R_{sd,c}(SOC_E, I, T) = (c_{c0}e^{-c_{c1}SOC_E} + c_{c2}) \cdot (c_{c3}I^{-c_{c4}} + c_{c5}) \cdot e^{c_{c6}\left(\frac{1}{T} - \frac{1}{T_{ref}}\right)} \\
C_{d,c}(SOC_E, I, T) = d_{c0}e^{-d_{c1}SOC_E} + d_{c2} \\
C_{sd,c}(SOC_E, I, T) = (e_{c0}e^{-e_{c1}SOC_E} + e_{c2}) \cdot e^{e_{c3}\left(\frac{1}{T} - \frac{1}{T_{ref}}\right)}
\end{cases}
\tag{25}
$$

The coefficients of the proposed battery model in the charge mode and the hybrid battery model are given in Table IV and V, respectively, for the test battery cells.

REFERENCES

[1] A. Eddahech, O. Briat, and J. Vinassa, "Real-time SOC and SOH estimation for EV Li-ion cell using online parameters identification," in *Proc. IEEE Energy Convers. Congr. Expo.*, Sept. 2012, pp. 4501-4505.

[2] S. M. Mousavi and M. Nikdel, "Various battery models for various simulation studies and applications," *Renewable and Sustainable Energy Reviews*, vol. 32, pp. 477-485, April 2014.

[3] E. Cortez, M. Moreno-Eguilaz, and F. Soriano, "Advanced methodology for the optimal sizing of the energy storage system in a hybrid electric fefuse collector vehicle using real routes," *Energies*, vol. 11, 3279, Nov. 2018.

[4] M. Farrokhabadi, S. König, C. A. Cañizares, K. Bhattacharya, and T. Leibrfied, "Energy storage system models for microgrid stability analysis and dynamic simulation," *IEEE Trans. Power Systems*, vol. 33, no.2, pp. 2301-2312, Mar. 2018.

[5] C. Zou, A. G. Kallapur, C. Manzie, and D. Nešić. "PDE battery model simplification for SOC and SOH estimator design," *in Proc. 54th IEEE Conf. Decision Control*, Dec. 2015, pp. 1328–1333.

[6] S. Rael and M. Hinaje, "Using electrical analogy to describe mass and charge transport in lithium-ion batteries," *J. Power Sources*, vol. 222, pp. 112-122, Jan. 2013.

[7] N. Lotfi, R. G. Landers, J. Li, and J. Park, "Reduced-order electrochemical model-based SOC observer with output model

uncertainty estimation," *IEEE Trans. Control Systems Technology*, vol. 25, no. 4, pp. 1217-1230, Jul. 2017.
[8] J. Marcicki, M. Canova, A. T. Conliks, and G. Rizzoni, "Design and parameterization analysis of a reduced-order electrochemical model of graphite/$LiFePO_4$ cells for SOC/SOH estimation," *J. Power Source*, vol. 237, pp. 310-324, Sept. 2013.
[9] J. Jaguemont, A. Nikolian, N. Omar, S. Goutam, J. V. Mierlo, and P. V. Bossche, "Development of a two-dimensional-thermal model of three battery chemistries," *IEEE Trans. Energy Convers*., vol. 32, no.4, pp. 1447-1455, Apr. 2017.
[10] K. Murashko, J. Pyrhonen, and L. Laurila, "Three-dimensional thermal model of a lithium ion battery for hybrid mobile working machines: Determination of the model parameters in a pouch cell," *IEEE Trans. Energy Convers*., vol. 28, no. 2, pp. 335-343, Jun. 2013.
[11] A. Seaman, T. Dao, and J. McPhee, "A survey of mathematics-based equivalent-circuit and electrochemical battery models for hybrid and electric vehicle simulation," *J. Power Sources*, vol. 256, pp. 410-423, Jun. 2014.
[12] C. R. Gould, C. M. Bingham, D. A. Stone, and P. Bentley, "New battery model and state-of-health determination through subspace parameter estimation and state-observer techniques," *IEEE Trans. Veh. Technol.*, vol. 58, no. 8, pp. 3905-3916, Oct. 2009.
[13] A. Hentunen, T. Lehmuspelto, and J. Suomela, "Time-domain parameter extraction method for Thevenin-equivalent circuit battery models," *IEEE Trans. Energy Convers.*, vol. 29, no. 3, pp. 558-566, Sept. 2014.
[14] K. Khan, M. Jafari, and L. Gauchia, "Comparison of Li-ion battery equivalent circuit modelling using impedance analyzer and Bayesian networks," *IET Electrical Systems in Transportation*, vol. 8, no. 3, pp. 197-204, Aug. 2018.
[15] J. Zhang, S. Ci, Sharif, and M. Alahmad, "An enhanced circuit-based model for single-cell battery," in *Proc.25th Applied Power Electronics Conference and Exhibition*, Feb. 2010, pp. 672-675.
[16] S. Tian, M. Hong, and M. Ouyang, "An experimental study and nonlinear modeling of discharge I-V behavior of valve-regulated lead-acid batteries," *IEEE Trans. Energy Convers*., vol. 24, no. 2, pp. 452-458, Jun. 2013.
[17] X. Tang, Y. Wang, C. Zou, K. Yao, Y. Xia, and F. Gao, "A novel framework for lithium-ion battery modeling considering uncertainties of temperature and aging," *Energy Convers. Management*, vol. 180, pp. 162-170, Jan. 2019.
[18] D. Rakhmatov, S. Vrudhula, and A. Wallach, "An analytical high-level battery model for use in energy management of portable electronic systems," in *Proc. Int. Conf. Computer Aided Design*, Nov. 2001, pp 488-493.
[19] T. Kim and W. Qiao, "A hybrid battery model capable of capturing dynamic circuit characteristics and nonlinear capacity effects," *IEEE Trans. Energy Convers.*, vol. 26, no. 4, pp. 1172-1180, Dec. 2011.
[20] J. F. Manwell and J. G. Mcgowan, "Lead acid battery storage model for hybrid energy system," *Solar Energy*, vol. 50, no. 5, pp. 399-405, May 1993.
[21] Y. Yamaguchi, M. Shiota, M. Hosokawa, Y. Nakayama, N. Hirai, and S. Hara, "Study of charge acceptance for the lead-acid battery through in situ EC-AFM observation--influence of the open-circuit standing time on the negative electrode," *J. Power Sources*, vol. 102, no. 1-2, pp. 155-161, Dec. 2001.
[22] S. S. Zhang, K. Xu, and T. R. Jow, "Study of the charging process of a LiCoO2-based Li-ion battery," *J. Power Source*, vol. 160, no. 2, pp. 1349-1354, Oct. 2006.
[23] T. Kim, Y. Wang, Z. Sahinoglu, T. Wada, S. Hara, and W. Qiao, "A Rayleigh quotient-based recurve total-least-square online maximum capacity estimation for lithium-ion batteries," *IEEE Trans. Energy Convers*., vol. 30, no. 3, pp. 842-851, Sept. 2015.
[24] Z. Gabriel, *Green Electrical Energy Storage*, Kindle Edition, Sept. 2016.
[25] T. Lambert, P. Gilman, and P. Lilienthal, "Micropower System Modeling with Homer," in *Integration of Alternative Sources of Energy*, John Wiley & Sons, 2006.
[26] J. F. Manwell, J. G. Mcgowan, U. Abdulwahid, and K. Wu, "Improvements to the hybrid2 battery model," in *Proc. Windpower Conf.*, May 2005, pp 1-22.
[27] X. Tang, X. Mao, J. Lin, and B. Koch, "Li-ion battery parameter estimation for state of charge," in *Proc. American Control Conf.*, Jun.-Jul. 2011, pp. 941-946.
[28] M. Verbrugge and E. Tate, "Adaptive state of charge algorithm for nickel metal hydride batteries including hysteresis phenomena," *J. Power Sources*, vol. 126, pp. 236-249, 2004.

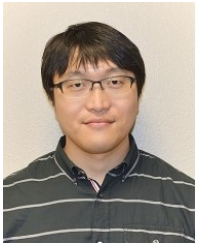

Taesic Kim (S'10–M'15) received the B.S. degree in Electronics Engineering from Changwon National University, Changwon, Korea, in 2008, and the M.S. degree in Electrical Engineering and the Ph.D. degree in Computer Engineering from the University of Nebraska–Lincoln, Lincoln, NE, USA in 2012 and 2015, respectively.

In 2009, he was with the New and Renewable Energy Research Group of Korea Electrotechnology Research Institute, Korea. In 2013, he was with Mitsubishi Electric Research Laboratories, Cambridge, MA, USA. Currently, he is an Assistant Professor in the Department of Electrical Engineering and Computer Science at the Texas A&M University–Kingsville. His research interests cover broad areas of cyber-physical power and energy systems including battery management systems, energy IoT, power electronics, and cyber-physical security.

He was the recipient of a 2018 Myron Zucker Student-Faculty Grant Award from the IEEE Foundation, the Best Paper Award of the 2017 IEEE International Conference on Electro Information Technology, and the First Prize Award of the 2013 IEEE Industry Applications Society Graduate Student Thesis Contest.

Wei Qiao (S'05–M'08–SM'12) received the B.Eng. and M.Eng. degrees in electrical engineering from Zhejiang University, Hangzhou, China, in 1997 and 2002, respectively, the M.S. degree in high-performance computation for engineered systems from Singapore-MIT Alliance, Singapore, in 2003, and the Ph.D. degree in electrical engineering from the Georgia Institute of Technology, Atlanta, GA, USA, in 2008.

Since August 2008, he has been with the University of Nebraska–Lincoln, Lincoln, NE, USA, where he is currently a Professor with the Department of Electrical and Computer Engineering. His research interests include renewable energy systems, smart grids, condition monitoring, power electronics, electric motor drives, energy storage systems, and emerging electrical energy conversion devices. He is the author or coauthor of more than 240 papers in refereed journals and conference proceedings.

Dr. Qiao is an Editor of the IEEE TRANSACTIONS ON ENERGY CONVERSION and an Associate Editor of the IEEE TRANSACTIONS ON POWER ELECTRONICS and the IEEE JOURNAL OF EMERGING AND SELECTED TOPICS IN POWER ELECTRONICS. He was the recipient of a 2010 U.S. National Science Foundation CAREER Award and the 2010 IEEE Industry Applications Society Andrew W. Smith Outstanding Young Member Award.

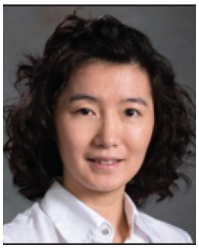

Liyan Qu (S'05–M'08–SM'17) received the B.Eng. (with the highest distinction) and M.Eng. degrees in electrical engineering from Zhejiang University, Hangzhou, China, in 1999 and 2002, respectively, and the Ph.D. degree in electrical engineering from the University of Illinois at Urbana–Champaign, Champaign, IL, USA, in 2007.

From 2007 to 2009, she was an Application Engineer with Ansoft Corporation, Irvine, CA, USA. Since January 2010, she has been with the University of Nebraska−Lincoln, Lincoln, NE, USA, where she is currently an Associate Professor with the Department of Electrical and Computer Engineering. Her research interests include energy efficiency, renewable energy, numerical analysis and computer aided design of electric machinery and power electronic devices, dynamics and control of electric machinery, and magnetic devices.

Dr. Qu was the recipient of a 2016 U.S. National Science Foundation CAREER Award.